Biophysical Chemistry 138 (2008) 91–98

Contents lists available at ScienceDirect

Biophysical Chemistry

journal homepage: http://www.elsevier.com/locate/biophyschem

Energetic contributions to the initiation of transcription in *E. coli*

Jayanthi Ramprakash, Frederick P. Schwarz *

Center for Advanced Research in Biotechnology/National Institute of Standards and Technology, 9600 Gudelsky Drive, Rockville, Maryland 20850, United States

ARTICLE INFO

Article history:
Received 23 July 2008
Received in revised form 2 September 2008
Accepted 3 September 2008
Available online 18 September 2008

Keywords:
Differential scanning calorimetry
DNA
Isothermal titration calorimetry
Promoters
RNA polymerase
Thermodynamics
Transcription

ABSTRACT

The thermodynamics of RNA polymerase (RNAP) binding to a 108 base pair (bp) synthetic promoter with consensus sequences at the −35 and −10 bp binding regions upstream from the transcription start point were determined using isothermal titration calorimetry (ITC). The binding constant at 25 °C is $2.37 \pm 0.18 \times 10^7$ M^{-1}, which is reduced to $0.17 \pm 0.06 \times 10^7$ M^{-1} with mutations in the −10 bp region but remained the same with mutations in the −35 binding region. The binding reactions were enthalpically-driven with exothermic binding enthalpies ranging from -57 ± 6 kJ mol^{-1} at 15 °C to -271 ± 20 kJ mol^{-1} at 35 °C yielding a large binding heat capacity change of -10.7 ± 1.9 kJ mol^{-1} K^{-1}, indicating a conformational change upon binding to the RNAP. Differential scanning calorimetry (DSC) scans of the thermal unfolding of RNAP and the promoter–RNAP complex exhibited an unfolding transition at 55.5 ± 0.6 °C and at 58.9 ± 0.5 °C for the RNAP but only one transition at 60.5 ± 1.1 °C for the complex with van't Hoff enthalpy to transition enthalpy ratios of, resp., 3.2 ± 0.3 and 4.3 ± 0.5. The single transition of the complex results from a shift to 60.5 °C of the low temperature transition upon promoter binding to the structural unit unfolding at the lower temperature in RNAP. The large transition enthalpy ratios indicate that the σ, α, α, β, and β′ subunits unfold as almost independent entities. The dissociation thermodynamics of short transcription "bubble" duplexes of 7 promoters sequenced from −1 to −12 bp were determined from ITC and DSC measurements. The free energy change of the promoter binding to the RNAP and the free energy requirement for formation of the transcription bubble at the low promoter concentrations in the cell are sufficient to drive the initiation of transcription through the isomerization of the closed to the open form step of the RNAP–promoter complex.

1. Introduction

The transcription of 300 promoter sequences in *E. coli* [1] is initiated by a sequence of thermodynamic events including the initial formation of a "closed" RNAP–promoter complex followed by isomerization to an "open" complex which includes unwinding of a subset of DNA sequences of the promoter near the transcription start point to form a transcription "bubble"[2]. The first step in this sequence of events is the binding of RNAP to the promoter principally at two sites on the promoter, a consensus TATAAT site centered at −10 bp and a consensus TTGACA site centered at −35 bp upstream from the transcription start point [1]. Nitrocellulose binding assays of the binding of a promoter to RNAP as a function of temperature show that the binding is accompanied by a large heat capacity change of -5.9 ± 1.3 kJ K^{-1}, implying a conformational change in the RNAP–promoter complex to align the DNA template onto the catalytic site of the RNAP [3]. The conformational change may occur exclusively in the RNAP or may be attributed to the bending of the promoter near the TATA box region, as observed in scanning force microscope images [4]. Dissociation of the sigma 70 (σ 70) subunit from the promoter–RNAP complex then occurs during isomerization of the "closed" complex to the open complex resulting in the formation of the transcription bubble to facilitate transcription of the promoter to messenger RNA. More specifically, the transcription bubble is formed by dissociation or "melting" of the complementary strands of the promoter from −12/−11 bp upstream to one or two bases downstream from the transcription start point and, thus, usually consists of almost the entire consensus TATAAT site centered at −10 bp upstream [5]. An interaction between T429 of the σ subunit of RNAP and a −11 A/T bp is believed to initiate separation of the DNA strands into the transcription bubble [5]. This kinetically-derived mechanism has been supported by FRET measurements [6] and by structural models developed from X-ray crystallographic data on the core enzyme from *Thermos aquaticus* [7] and on yeast RNA polymerase [8]. The proposed structural model involves the ββ′ and αα′ subunits of RNAP and consists of inserting the promoter in a cleft in the RNAP formed by the ββ′ subunits and the N-terminal domains of the αα′ subunits so that the transcription bubble formed on the promoter is in contact with the catalytic site of the ββ′ subunits at the bottom of the cleft [7,8]. The catalytic site then employs the single strand DNA template of the transcription bubble to generate a RNA sequence complementary to the single DNA strand. The isomerization of the initiation complex to the open complex form occurs when the transcription bubble is formed and is then followed by elongation, termination, and editing of the RNA transcript as described earlier in terms of a qualitatively-integrated thermodynamic, kinetic, and

* Corresponding author. Tel.: +1 240 314 6219.
E-mail address: fred@carb.nist.gov (F.P. Schwarz).

0301-4622/$ – see front matter © 2008 Elsevier B.V. All rights reserved.
doi:10.1016/j.bpc.2008.09.007

structural model [9]. Remarkably, all of these processes of promoter binding and formation of the transcription bubble upon isomerization to the open initiation complex are solely driven by the binding free energy and not by coupled hydrolysis reactions as is hypothesized for other biological processes [10].

In this investigation, the thermodynamic events accompanying the formation of the open form of the initiation complex are determined quantitatively from calorimetry measurements. The binding thermodynamic parameters of a synthetic 108 bp consensus *lace* promoter with consensus binding sequences centered at −10 bp and −35 bp upstream from the transcription start point (*sync on* promoter), as shown in Fig. 1, were determined as a function of temperature and of sequence changes in the −35 bp and −10 bp RNAP-binding regions using ITC. Any implied conformational changes in RNAP upon binding of the promoter to form the closed complex were explored by comparing the DSC results on the thermal unfolding of the free RNAP to the thermal unfolding of the RNAP–*syncon* promoter complex. Differences in the thermodynamic requirements for the formation of the transcription bubble from separation of the DNA strands of the three 108 bp *syncon* promoters between the transcription start point at +1 bp and −13 bp were determined from DSC results on the thermal dissociation of the short 12 bp transcription bubble duplexes. Short 12 bp bubble duplexes of four additional promoters with different rates of formation of the promoter–RNAP complex [11], as listed in Table 1, were also included in this investigation. The DSC results were compared to the ITC results on the formation of the 12 bp duplexes. The length of the transcription bubble duplexes employed in this investigation was based on several considerations. It was observed that for *bacillus subtitles* sigma RNAP bound to the *flagellant* promoter that the transcription bubble extends from the −10 bp region to near −1 bp at 20 °C and to +3 bp at 40 °C facilitated by the presence of nucleoside triphosphates and Mg^{+2} [12]. The formation of the transcription bubble of the *spollG* promoter [13] by *bacillus subtilis* sigmaD RNAP was hypothesized to occur in two steps with first formation or "melting" between −13 bp and −3 bp of the promoter in the absence of nucleotides followed by extension to the +1 bp start point in the presence of nucleotides. Similarly, the formation of the

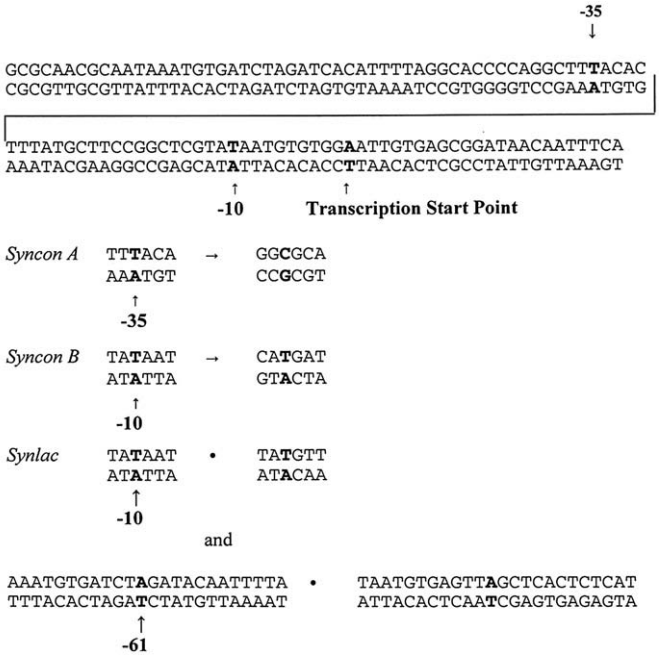

Fig. 1. Sequences of the promoters used in the RNAP binding measurements. *Syncon* A is a −35 bp region mutant of the *syncon* promoter. *Syncon* B is a −10 bp region mutant of the *syncon* promoter with two separated mutations. *Synlac* is a −10 bp region mutant of the *syncon* promoter with two adjacent mutations.

Table 1
Promoter transcription "bubble" duplexes

Promoter	Sequence	Rate of RNAP complex formation 10^8 M^{-1} s^{-1}
P_{tac} or P_{sc} P_{sc}[a]	TATAATGTGTGG ATATTACACACC	0.85
P_L[a]	GATACTGAGCAC CTATGACTCGTA	0.10
P_{con}[a]	TATAATGGTACC ATATTACCATGG	1.1
P_{bla}[a]	GACAATAACCCT CTGTTATTGGGA	0.10
P_{N25}[a]	TATAATAGATTC ATATTATCTAAG	2.9
P_{sb}	CATGATGTGTGG GTACTACACACC	
P_{slac}	TATGTTGTGTGG ATACAACACACC	

The bases in the bold letters are at the −10 position on the promoter.
[a] These sequences are from reference [11].

transcription bubble by *E. coli.* RNAP is believed to proceed initially with nucleation or localized melting of the promoter near −11 bp and is then followed by extending the incompletely initially-formed bubble to a final fully developed transcription bubble [5]. In addition, different start points for transcription have been observed for many promoters in *E. coli.* [14] and so RNAP may be somewhat flexible in the extension of the transcription bubble starting from localized melting of the promoter near −11 bp. Accordingly, in this investigation, the promoter DNA duplexes chosen to compare the thermodynamic requirements for the initial formation of the transcription bubble in the absence of the nucleoside triphosphates and Mg^{+2} were promoter sequences from −1 bp to −13 bp. In fact, short 14 bp promoter duplex fragments consisting of only the −10 consensus sequence have also been shown to undergo melting at temperatures above 14 °C when bound to RNAP [10]. All the promoter sequences employed in this investigation contained the critical −11 A/T bp [4,15] and lacked mutations at −7, which would significantly affect the binding affinity to RNAP [10]. These different thermodynamic contributions to the initiation of transcription are then discussed in terms of the thermodynamic requirements for the initiation of transcription in *E. coli.*

2. Experimental

2.1. Materials

The RNAP was prepared and purified according to the procedure described by Lowe et al. [16] and an extinction coefficient of 2.77×10^5 cm^{-1} M^{-1} at 280 nm was used to determine the concentration of the RNAP, although not all of the RNAP in the sample was active to bind the promoters [17]. The enzyme activity of the RNAP was checked by following the protocol described by Zhang et al. [18] which employs a 10 min pre-equilibrated 25 μL reaction mixture consisting of 0.5 nM of a 203-bp *lac* operon, 40 nM of the purified RNAP, 50 nM [α-^{32}P]UTP from Amersham Pharmacia Biotech, and 200 μM cNMP in a buffer consisting of 40 mM tris[Hydroxymethyl]aminoethane (tris)–HCl at pH=8.0 containing 100 mM KCl, 10 mM $MgCl_2$, 2 mM mercaptoethanol, and 5% glycerol at 37 °C. The enzyme reaction was initiated by the addition of ApA to the mixture at a concentration of 0.25 mM ApA and then allowed to proceed for 15 min. The reaction was terminated by the addition of 25 μL of a solution of 80% formamide, 89 mM Tris, 89 mM boric acid, 2 mM EDTA, 0.05% bromphenol blue, and 0.05% xylene cyanol. The reaction product, [α-^{32}P]AAUU, was resolved by electrophoresis on a 20% polyacrylamide and 8 M urea gel and quantified by using a storage phosphor autoradiography method in conjunction with a Molecular Dynamics 300 E Phosphor Imager equipped with Image Quant software. The RNAP core was obtained from Epicentra Biotechnologies and the original concentration of

0.7 g L^{-1} as stated by the supplier was taken as the concentration of the RNAP core after it was dialyzed in the phosphate buffer described below for the RNAP ITC binding measurements. The 108 bp *syncon* promoter was from −82 to +22 of the *lacUV5* promoter, so that it contained the principal RNA polymerase binding site sequences at −10 bp and −35 bp and 108 bp promoters with mutations at −10 bp and −35 bp, as shown in Fig. 1.

Each complementary strand of the 108 bp promoter was synthesized on the μmol level on a DNA synthesizer and purified by gel electrophoresis. The complementary sequences were annealed by heating equal amounts of each strand in 10 mM tris–HCl buffer containing 1 mM $MgCl_2$ and 0.5 M NaCl at pH = 7.4 up to 95 °C followed by slow cooling down to room temperature. The concentration of the 108 bp *syncon* promoters was determined from OD measurements at 260 nm using an extinction coefficient of 1.3×10^6 cm^{-1} M^{-1} based on an OD of 1 for a 50 ng μL^{-1} solution [19] and a molecular mass of 65,000 g mol^{-1}. The ITC promoter to RNAP binding measurements were performed in phosphate buffer consisting of 50 mM K_3PO_4 and contained 0.2 mM dithiothreitol (DTT), 0.2 mM ethylenediamine (EDTA), and 0.15 mM KCl at pH = 7.0. The potassium phosphate salts, sodium chloride, potassium chloride, tris, DDT, and $MgCl_2$ were reagent grade from Sigma Chemical Co. The DTT was ultra pure brand from GIBCOBRL. The sodium salt of EDTA was from Serva Co. The HCl and glycerol were reagent grade from Mallinckrodt.

The lyophilized synthetic 12mer single strand DNA sequences were obtained from two sources, Oligos, Etc. and Integrated DNA Technologies, de-salted and HPLC purified and used without any further purification. The ITC binding experiments between the DNA complementary strands were performed in 10 mM sodium phosphate + 1 mM EDTA at pH = 7.0 buffer. The concentration of the ssDNA was determined by UV absorption measurements at 260 nm and use of the extinction coefficients from the supplier. DSC melting scans were performed on the resulting DNA duplexes from the ITC measurements. DSC scans were also performed on the ssDNA sequences to determine if they are stacked at ambient temperatures.

2.2. Isothermal titration calorimetry

The binding constants and binding enthalpies for the 108 bp *syncon* promoter mutants binding to RNAP and for formation of the short promoter DNA duplexes were determined from ITC measurements, using a Microcal, Inc. VP Titration Calorimeter as described previously [20]. The reference solution vessel contained the dialysate and the sample vessel contained 1 to 3 μM RNAP in the potassium phosphate buffer solution and 2–4 μL aliquots of the 0.03 to 0.1 mM *syncon* or mutant promoter in the potassium phosphate buffer solution were titrated 3 to 4 min apart into the RNAP solution until the binding to RNAP was saturated as evidenced by the lack of a heat exchange signal. (The ribonucleotide triphosphate reactants and Mg^{+2} were absent from the solution.) Prior to the promoter into RNAP solution titration, 2–4 μL aliquots of the promoter solution was titrated into the dialysate in the sample vessel to determine any heats of dilution of the promoter solution. The same procedure was followed for the formation of the transcription bubble duplexes where 5 μL aliquots of 0.1 to 1.0 mM short promoter DNA sequences were titrated into 10 to 20 μM solutions of their complementary sequences in 10 mM sodium phosphate buffer at pH 7.0 with 1.0 mM EDTA. The same buffer was in the reference vessel of the ITC.

Analysis of the titrations consisted first of subtracting an average heat of dilution of the titrant (promoter or DNA solution) from their corresponding binding isotherms where the total integrated heat exchanged as a function of the total number of moles of titrant are plotted as a function of the ratio of the moles of titrant to the number of moles of reactant in the sample vessel of the ITC. A single-site binding model equation is then fitted to the resulting binding isotherms to determine values for $\Delta_b H$, K_b, and n, the amount of moles of titrant to the amount of moles of reactant in the sample vessel at half the saturation of the reactant in the sample vessel, as described previously [20]. The fitting procedure was performed by the software program Origin from Microcal, Inc. It was found that fits of a single-site binding site model to the promoter binding to RNAP isotherms yielded binding constants and enthalpies that were dependent on the concentration of the promoter titrant in the stirrer syringe but independent of the approximate concentration of active RNAP in the sample solution. Accordingly, the n values of the promoter to RNAP binding reactions are not recorded. Values of the binding free energy change ($\Delta_b G^0$) and the binding entropy ($\Delta_b S^0$) were then determined from the fundamental equation of thermodynamics:

$$\Delta_b G^0 = -RT \ln \{K_b\} = \Delta_b H^0 - T\Delta_b S^0 \quad (1)$$

The heat capacity change for the binding reaction, $\Delta_b C_p$, was determined as the slope of the assumed linear dependence of the binding enthalpy on temperature.

Uncertainties in n, K_b, and $\Delta_b H^0$ for each ITC scan were generated from the final iterative fit of the single-site binding model to the ITC isotherm data. Each ITC reaction was performed at least twice and the uncertainties in the values of n, K_b, and $\Delta_b H^0$ of each ITC scan were employed as weighing factors in determining average values for n, K_b, and $\Delta_b H^0$ from the ITC reactions. The uncertainties are, thus, reported as standard deviations of the average n, K_b, and $\Delta_b H^0$ values.

2.3. Differential scanning calorimetry

A VP-DSC Microcalorimeter from Microcal, Inc. (Northampton, MA) was employed for the DSC measurements. The DSC consists of a matched pair of 0.511 mL sample and reference vessels. In a series of DSC scans, both vessels were first loaded with the buffer solution, equilibrated for 15 min at a pre-set temperature of 25 °C and scanned up to 95 °C at a pre-set scan rate. The buffer versus buffer scan was repeated once for a second scan following cooling of the first scan. After cooling of the second scan, the sample vessel was then emptied and loaded with the transcription bubble DNA or the RNAP solution by means of a syringe and prior to the 15 min equilibration period at the lower temperature. The RNAP solutions were scanned at pre-set scan rates from 15 to 90 °C h^{-1} to determine any dependence of the RNAP transition parameters on DSC scan rate, whereas the reversible DNA duplex solutions were scanned only at 60 °C h^{-1}. The solution scans were repeated several times to determine if the transitions were reversible. After completion of a set of scans, the second buffer versus buffer scan was used as the baseline scan and subtracted from each of the solution versus buffer scans for analysis. The net solution versus buffer scan was converted to a heat capacity versus temperature scan and the DNA duplex and RNAP transitions were analyzed in terms of a two-state thermodynamic transition model by using the EXAM software program [21]. The EXAM program [21] employs a sigmoidal baseline, which follows the profile of the transition peak for extrapolation of the pre- and post-transitional baselines under the transition peak to determine the transition peak area, the transition van't Hoff enthalpy ($\Delta_{trs}H_{vH}$) and the transition temperature (T_G) where the transition peak area is half of the total area. The transition van't Hoff enthalpy is determined from $d(\ln\{K(T)\})/d(1/T)$ where the transition equilibrium constant, $K(T)$ is determined from the fractional area, $\alpha(T)$ up to a temperature T. The ratio of the transition peak area to the amount of RNAP or DNA duplex in the sample vessel yielded values for the transition enthalpy ($\Delta_{trs}H$). The RNAP transitions were analyzed in terms of a two-state A↔B transition model by using EXAM. The dissociation or "melting" of the transcription "bubble" DNA duplexes was analyzed in terms of a $A_2 \leftrightarrow 2B$ two-state thermodynamic transition model to yield the dissociation temperature of the duplex (T_d), the dissociation enthalpy ($\Delta_d H_{vH}$) in terms of change of enthalpy per duplex, and the dissociation enthalpy ($\Delta_d H$) from the area of the

dissociation transition to the number of modes of duplex in the DSC sample. Although the dissociation of the DNA duplex to its complementary strands is best represented by AB↔A+B, the A_2↔2B dissociative model was used since whether or not the products are identical, the profiles of the transition peak are the same [21], and so are values of the transition temperature and the van't Hoff dissociation enthalpies [21,22]. The uncertainties in the transition temperatures, the van't Hoff enthalpies, and the transition/dissociation enthalpies were determined as standard deviations of the average values of repeated DSC scans of the samples.

The binding constants determined from the ITC measurements were extrapolated up to the transition temperatures of the RNAP and employed to estimate the increase in the denaturation temperature of each transition in its complexed state since the *syncon* promoter does not bind to the unfolded state [23]. The equations utilized for the above calculations are as follows for extrapolation of the ITC determined binding constants up to the transition temperature of the RNAP–promoter complex, $T_G(P)$,

$$\ln[K_b(T_G(P)/K(T_o)] = [(-\Delta_b H(T_o) + \Delta_b C_p T_o)/R](1/T_G(P) - 1/T_o) + (\Delta_b C_p/R)\ln(T_G(P)/T_o) \quad (2)$$

and for estimates of the temperature shifts at the denaturation temperature,

$$1/T_G - 1/T_G(P) = (R/\Delta_{trs}H)\ln\{1.00 + ([P_o] - [RNAP_o]/2)K_b(T_G(P))\} \quad (3)$$

where T_o is the temperature of ITC determinations of K_b, T_G is the transition temperature of each transition of the RNAP alone, $T_G(P)$ is the transition temperature of the complex, $\Delta_{trs}H$ is the transition enthalpy of the complex, $[P_o]$ is the total initial promoter concentration, and $[RNAP_o]$ is the total initial RNAP concentration [23].

The DSC enthalpies on the dissociation of the shorter transcription bubble duplexes listed in Table 1 can be compared to the ITC enthalpies on the formation of the transcription DNA bubble sequences since any heat capacity change upon formation of the transcription bubble duplexes will be shown by ITC to be negligible. For thermodynamic comparison of the dissociation of the transcription bubble duplexes at 25 °C,

$$\Delta_d G^o(T) = T/T_d\{\Delta_d G^o(T_d)\} - \Delta_d H^o(T_d)\{1 - T/T_d\} \quad (4a)$$

where, for non-identical complementary DNA sequences at the dissociation temperature,

$$\Delta_d G^o(T_d) = -RT_d \ln\{4/C_t\} \quad (4b)$$

T=298.15 K, T_d=dissociation temperature in K, and /C_t is the total ssDNA strand concentration [22]. The dissociation temperatures of the transcription bubble duplexes are defined as the temperature where 50% of the duplex is dissociated into ssDNA and decrease with decrease in concentration as shown by the following

$$\mathrm{Ln}\{[DNA]_h/[DNA]_l\} = -\Delta_d H/R(1/T_d([DNA]_h) - 1/T_d[DNA]_l)) \quad (5)$$

where $[DNA]_h$ is a high concentration of DNA and $[DNA]_l$ is the low concentration of DNA. The reciprocal of the temperature shift, $\delta(1/T)$ is then

$$\delta(1/T) = (1/T_d([DNA]_h) - 1/T_d[DNA]_l) = -R/\Delta_d H \mathrm{Ln}\{[DNA]_h/[DNA]_l\} \quad (6)$$

However, it should be emphasized that Eqs. (5) and (6) are uniquely applicable to short DNA duplexes and not necessarily to long oligomers such as promoters [22].

3. Results

A typical ITC titration of 5 μL aliquots of 0.115 mM *syncon* promoter into approximately 1.5 μM RNAP solution at 25.0 °C is shown in Fig. 2.

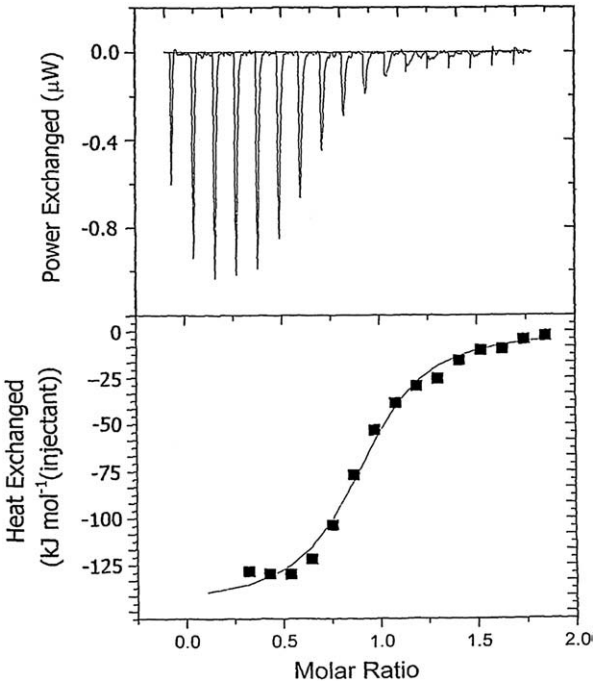

Fig. 2. An ITC titration of 5 μL aliquots of a 0.115 mM *syncon* promoter solution into 1.5 μM RNAP at 25 °C (upper panel). The binding isotherm of the titration is shown along with a fit (solid line) of a 1:1 binding model of the promoter to RNAP (lower fit).

The ITC results on the binding of the *syncon* promoter and its mutated *syncon A*, *synlac*, and *syncon B* forms to RNAP are summarized in Table 2. The binding reactions are exothermic and enthalpically-driven with the RNAP binding constants ranging from $0.17 \pm 0.06 \times 10^7$ M^{-1} for the *syncon B* promoter with 2 separated mutations in the −10 bp region to $2.37 \pm 0.18 \times 10^7$ M^{-1} for the *syncon* promoter at 25.0 °C and binding enthalpies ranging from −131 ± 13 kJ mol^{-1} for the *syncon* promoter to −73 ± 3 kJ mol^{-1} for the *syncon A* promoter at 25.0 °C. The binding constant of the *synlac* promoter with 2 adjacent mutations in the −10 bp region is $1.73 \pm 0.50 \times 10^7$ M^{-1}, also lower than that of the *syncon* promoter. The binding constant of the *syncon* promoter is close to the binding constant of $2.7 \pm 0.4 \times 10^7$ M^{-1} determined from a nitrocellulose assay at 28 °C for Pλ 861 bp promoter binding to RNAP [3]. The Pλ promoter differs from the *syncon* promoter at the −10 bp and −35 bp RNAP binding regions by TTGACT-17 bp-GATAAT for the Pλ promoter compared to TTTACA-18 bp-TATAAT for the *syncon* promoter, a difference of only 1 bp in the −10 region and two bps in the −35 region. The binding constants of the *syncon* promoter and its *syncon A*, the −35 bp region mutant, are the same to within experimental error while the binding constant of *syncon B*, the −10 bp region mutant, is an order of magnitude lower than the *syncon* promoter binding constant. There is also a reduction in the *synlac* binding constant to $1.73 \pm 0.50 \times 10^7$ M^{-1} at 25.0 °C resulting from mutations in the −10 bp region. (The mutations in the −61 bp region are not involved in the binding reaction to RNAP.) The binding constants of the *syncon* promoter exhibit an increase with increase in temperature as is observed with the Pλ promoter with binding constants of $2.1 \pm 0.9 \times 10^7$ M^{-1} at 7.3 °C and $4.6 \pm 0.8 \times 10^7$ M^{-1} at 25.0 °C but for the Pλ promoter there is a decrease to $5.8 \pm 2.6 \times 10^6$ M^{-1} at 37 °C [3]. A linear plot of the binding enthalpy versus temperature for the *syncon* promoter yields a large heat capacity change of $\Delta_b C_p = -10.7 \pm 1.9$ kJ $mol^{-1}K^{-1}$, higher than the reported heat capacity change of −5.9 ± 1.3 kJ mol^{-1} K^{-1} for binding of the Pλ promoter to RNAP determined from nitrocellulose binding assays [3]. Since almost all experimental values are statistically within three sample standard deviations of the mean value, the literature value of −5.9 ± 1.3 kJ mol^{-1} K^{-1} may be considered within the acceptable data set for the heat capacity change of −10.7 ± 1.9 kJ mol^{-1} K^{-1}. This

Table 2
Thermodynamic parameters for promoter binding to RNAP from ITC

Promoter	T	$K_b \times 10^7$	$-\Delta_b G^o$	$-\Delta_b H^o$	$-T\Delta_b S^o$
	°C	M^{-1}	kJ mol^{-1}		
Syncon	15.0	1.59±0.44	39.7±0.7	57±6	17±2
Syncon	25.0	2.37±0.18	42.1±0.2	131±13	89±9
Synlac	25.0	1.73±0.50	41.3±0.7	84±4	43±2
Syncon A	25.0	2.07±0.18	41.7±0.2	73±3	31±1
Syncon B	25.0	0.17±0.06	35.5±0.9	110±19	84±17
Syncon	35.0	2.88±0.59	44.0±0.5	271±20	227±23
			Syncon $\Delta_b C_p = -10.7 \pm 1.9$ kJ mol^{-1} K^{-1}		

See Fig. 1 for the DNA sequences of the promoters.

large heat capacity change may be attributed to a bending of the promoter [5] bound to RNAP or to a conformational change in the RNAP upon binding to the promoter [3].

To determine if there are any conformational changes of the RNAP in going from the unbound state to the closed complex with the promoter, the unfolding thermodynamic quantities of RNAP were compared to the unfolding thermodynamic quantities of the RNAP–promoter complex using DSC. Typical DSC scans of a 0.43 μM RNAP solution and the RNAP bound to the *syncon* promoter at a concentration of 0.96 μM are shown in Fig. 3. In Fig. 3, the DSC scan rate was 60 K h^{-1} and the thermodynamic quantities describing the transitions were found to be independent of scan rate from 15 K h^{-1} to 90 K h^{-1}, as also shown in Table 3. The transitions did not re-appear upon a re-scan of the solution but the thermodynamic transition quantities determined from a least squares fits of a two-state transition model to the DSC data were found to be independent of the DSC scan rate in Table 3. Since the transition thermodynamic properties are independent of scan rate, Manley et al. have shown that, even though they appear to be irreversible, they can still be analyzed by a thermodynamic two-state transition model [24]. Although the transition peaks at each temperature could be a superposition of several two-state transitions centered at each temperature, the transitions at each temperature were analyzed in terms of single A↔B two-state transitions to determine basically if there were any large conformational differences between the unbound RNAP and the *syncon* promoter–RNAP complex. The single transition enthalpies and temperatures were found to be independent of the RNAP concentration from 0.72 to 2.0 μM indicating the absence of any association of the RNAP at and below the 2.0 μM level (Table 3). The DSC results in Fig. 3 exhibit a change in the thermodynamics of the unfolding transitions so that the two transition peaks in the unbound RNAP merge into a single transition at a higher temperature for the *syncon* promoter–RNAP complex. Continued scanning of the *syncon* promoter–RNAP complex up to 95 °C resulted in a second transition peak at 81.6 °C with a transition enthalpy of 2900 kJ mol^{-1}. This second transition re-appeared upon a re-scan of the sample and was also observed at the same transition temperature in samples of just the *syncon* promoter solutions. It arises from the dissociation ("melting") of the *syncon* promoter into its complementary DNA sequences at 81.6 °C. The thermodynamic quantities describing the thermal unfolding transitions of RNAP are summarized in Table 3. Ratios of the transition enthalpies to van't Hoff enthalpies for the RNAP and the *syncon* promoter–RNAP complex solutions are from 3.2 to 3.8 and indicate almost independent unfolding transitions of thermodynamic domains of the RNAP. RNAP in the unligated state consists of 2α, 2β, and 1σ subunit, a total of 5 structural subunits and, however, binding to the promoter releases the σ subunit from RNAP. The unfolding transitions observed for RNAP can tentatively be identified with the unfolding transitions of the 5 structural subunits of RNAP where two or more of the structural subunits of RNAP interacting strongly to unfold as a single entity. Two unfolding transitions are also exhibited by the uncomplexed core RNAP that contains all of the structural subunits of RNAP with the exception of the σ structural subunit. The thermodynamic quantities of the unfolding transition of the uncomplexed core RNAP are also summarized in Table 3. The single transition of the *syncon* promoter–RNAP complex arises from enhanced thermal stabilization of the RNAP domain or domains at the lower temperature transition of 55.5±0.6 °C in the native state upon binding to the promoter. (The higher temperature transition is almost within experimental error of the temperature of the single *syncon* promoter–RNAP transition.) Applying Eqs. (2) and (3) to the DSC results from a solution of 0.43 μM RNAP complexed with 0.96 μM *syncon* promoter (Fig. 3) yields a predicted temperature increase to 63.7±0.6 °C for this transition, which is within 2× the experimental uncertainty of the transition temperature of 60.5±1.1 °C for the complex, i.e. a predicted lower limit of 62.5 °C versus an upper experimental value of 62.7 °C. The lower-temperature transition can be identified with unfolding of the ββ′ subunits, which contain the catalytic site and act as the cleft for insertion of the promoter [7,8]. Accordingly, the high temperature transition in the uncomplexed RNAP is unaffected by the presence of the promoter and can be identified with unfolding of the αα' subunits that act as the hinge of the cleft.

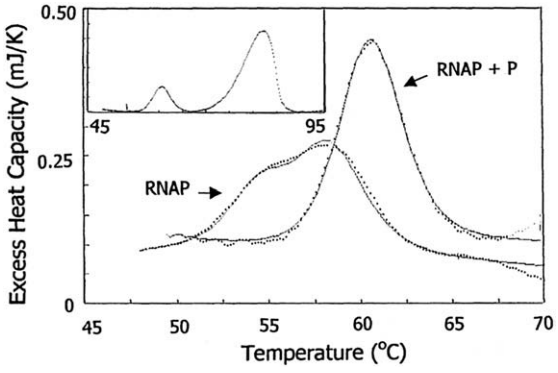

Fig. 3. A DSC scan of 0.43 μM RNAP alone and of a sample of 0.43 μM RNAP complexed with 0.96 μM *syncon* promoter shown as data points and least squares fits of two-state A↔B transition models to the data shown as solid lines. The inset shows the dissociation transition of the 0.96 μM *syncon* promoter in the sample.

Table 3
Thermodynamic parameters of the thermal denaturation of RNAP from DSC

RNAP concentration	*Syncon* promoter concentration	Scan rate	T_G	$\Delta_{trs}H_{vH}$	$\Delta_{trs}H$	$\Delta_{trs}H/\Delta_{trs}H_{vH}$
μM	μM	$K\,h^{-1}$	°C	kJ $mol-1$		Ratios
0.72 to 2.0	0	60	58.9±0.5	764±40	2500±200	3.2±0.3[a]
			55.5±0.6	794±53		
	0	90	59.5±0.5	724±36	2504±125	3.3±0.2[a]
			55.4±0.05	787±39		
	0	15	57.8±0.5	580±58	2293±115	3.5±0.4[a]
			53.8±0.5	745±37		
0.78 to 2.0	1 to 4	60	60.5±1.1	756±112	2900±240	3.8±0.6
		90	62.4±1.0	641±32	2764±138	4.3±0.2
		15	59.6±1.0	670±10	3214±160	4.8±0.2
1.9 core	0		56.9±1.0	584±60	1643±164	2.8±0.4
	0		51.9±1.0	556±60		

[a]The ratio was determined as the ratio of the average van't Hoff enthalpy of the two transitions to the total calorimetric enthalpy.

A typical ITC titration consisting of 5 μL aliquots of a 0.81 mM of a 5′TATAATGTGTGG3′ DNA solution injected into 40 μM of its complementary sequence, 5′CCACACATTATA3′, solution at 25.0 °C is shown in Fig. 4. The resulting transcription "bubble" duplex sequence formed from this titration is of the P_{tac} promoter that has the same sequence between the transcription start point and the −10 region as that of the *syncon* promoter. The results of a least squares fit of a single-site binding model to the binding isotherm are shown by the solid line in the lower panel of Fig. 4. Similar thermodynamic binding parameters for the transcription bubble duplexes presented in Table 1 are summarized in Table 4. The stoichiometries of the binding reactions are close to one and start decreasing with increase in temperature,

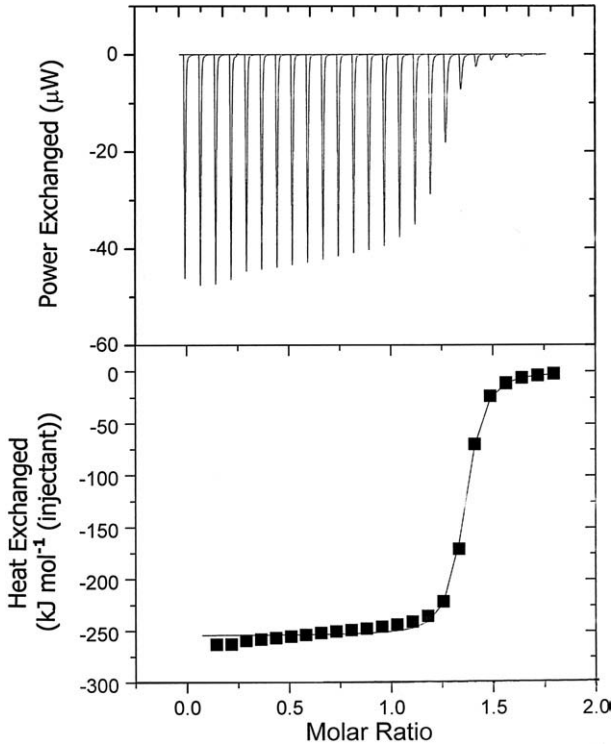

Fig. 4. An ITC titration of 5 μL aliquots of 0.81 mM TATAATGTGTGG into 0.04 mM CCACACATTATA at 25 °C (upper panel). The binding isotherm of the titration along with a least squares fit (solid line) of a 1:1 binding model to the binding isotherm (lower panel).

probably as a consequence of the onset of dissociation of the duplexes at the higher temperatures. The binding constants vary by more than an order of magnitude at 25 °C, from $0.76\pm0.05\times10^6$ M^{-1} for P_{N25} to $22.4\pm3.4\times10^6$ M^{-1} for P_{tac}, and these differences may be partially responsible for differences in the *in vivo* rate of RNA synthesis [11] since the separation of the duplexes to form the transcription bubble is one of the steps in the initiation of transcription. The binding constants and enthalpies from 25 °C to 35 °C are in the same range of values as those determined for the formation of 10 bp DNA duplexes [25]. The binding enthalpies are independent of temperature from 25 to 35 °C so that over this temperature range there is no heat capacity change for the formation of the DNA duplex. This lack of a heat capacity change is also derived from the dependence of $\ln\{K_b\}$ on $1/T$ with slopes that yield values for Δ_bH_{vH} that overlap with the direct values of Δ_bH determined from the ITC measurements. (These values are not presented in Table 4 because they are based on only 3 temperatures and yield large uncertainties of up to 50%.) The lack of any heat capacity change upon binding of the complementary DNA sequences also emphasizes the simplified form of Eqs. (4a) and (4b) that neglect heat capacity changes.

Table 4
Thermodynamic binding parameters of transcription "bubble" DNA sequences to their complement sequences at pH 7.0 from ITC results

Promoter	n	K_b	$-\Delta_bG$	$-\Delta_bH$	$-T\Delta_bS$
		$\times10^7$ M^{-1}	kJ mol^{-1}		
At 25 °C					
P_{tac}	1.15±0.01	2.24±0.34	42.0±0.4	288±38	246±38
P_L	0.75±0.01	1.99±0.19	41.7±0.2	350±26	308±26
P_{sb}	0.85±0.05	1.52±0.24	41.0±0.4	313±4	272±3
P_{slac}	1.06±0.01	0.583±0.043	38.6±0.2	336±6	297±6
P_{con}	1.07±0.01	0.581±0.068	38.6±0.3	223±19	184±19
P_{bla}	1.28±0.01	0.538±0.043	38.4±0.2	323±25	285±25
P_{N25}	1.09±0.01	0.0755±0.0048	33.6±0.2	266±22	232±22
At 30 °C					
P_{tac}	0.78±0.01	1.12±0.17	40.9±0.4	335±33	294±33
P_L	0.97±0.01	1.06±0.09	35.0±0.2	340±18	305±18
P_{sb}	0.90±0.02	0.329±0.011	37.8±0.1	310±8	272±3
P_{slac}	0.81±0.02	0.143±0.010	35.7±0.2	347±2	311±3
P_{con}	0.79±0.01	0.373±0.091	38.1±0.6	277±66	239±66
P_{bla}	0.75±0.01	0.110±0.25	35.1±0.6	414±96	379±99
At 35 °C					
P_{tac}	1.09±0.01	0.345±0.012	38.6±0.1	282±7	243±7
P_L	0.99±0.01	0.0700±0.027	34.5±1.0	349±9	314±9
P_{sb}	0.91±0.04	0.0488±0.0042	33.6±0.3	330±7	296±6
P_{slac}	1.23±0.04	0.0203±0.0010	35.7±0.2	360±5	324±5
P_{con}	0.88±0.01	0.0091±0.0009	35.2±0.2	267±39	232±39
P_{bla}	0.63±0.03	0.0085±0.0019	35.0±0.6	509±54	474±54

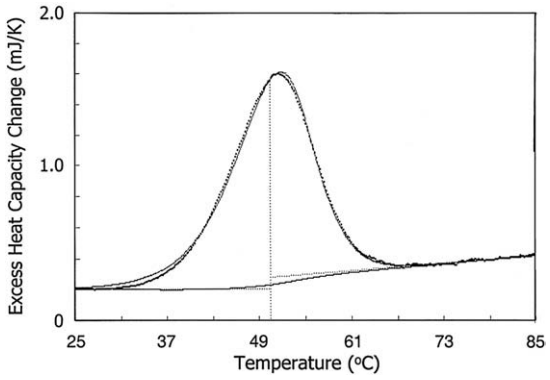

Fig. 5. A DSC scan of a 0.120 mM P_{tac} solution shown by the data points and a least squares fit of a two-state $A_2\leftrightarrow2B$ transition model to the data shown by the solid line. The broken vertical line indicates the dissociation temperature determined from the fit.

The ITC results in Table 4 are compared to the dissociation thermodynamics of the transcription bubble duplexes into separate single strand DNA determined from DSC. A typical DSC scan is presented in Fig. 5 for the dissociation of 0.120 mM of the P_{tac} promoter transcription "bubble" duplex at a scan rate of 60 K h^{-1}. The dissociation transitions re-appeared upon a re-scan of the sample. The result of a fit of a dissociative $A_2\leftrightarrow2B$ transition model to the DSC data is shown for the 0.120 mM P_{tac} solution by the solid line in Fig. 5. The thermodynamic parameters from fits of this model to the DSC dissociation scans of the other promoters are summarized in Table 5. The dissociation temperatures range from 34.5±0.5 °C for P_{N25} to 56.9±0.7 °C for P_L but are not in the same order as the association constants at 25 °C, probably resulting from some contributing thermodynamic parameters from partial stacking of the single strands at 25 °C [26,27]. The ratios of the transition enthalpies determined from the duplex concentrations to the van't Hoff enthalpies at high concentrations are between 0.5 and 1.0 where 1.0 would be expected from dissociation of the duplex into two complementary strands. Calculated values for T_d based on the high concentration results using

Table 5
Thermodynamics of the dissociation of the transcription "bubble" promoter duplexes from DSC results

Promoter	Concentration	T_d	Calculated T_d[a]	Δ_dH_{vH}	Δ_dH	Δ_dH/Δ_dH_{vH}
	mM	°C		kJ mol^{-1}		
P_L	0.134	56.9±0.7		427±5	231±4	0.54±0.01
	0.009	49.3±0.3	46.7	394±4	237±6	0.60±0.02
P_{bla}	0.112	52.8±0.1		389±7	273±7	0.70±0.04
	0.011	46.5±0.6	45.5	337±20	210±4	0.62±0.04
P_{tac}	0.120	50.0±0.1		400±48	328±11	0.82±0.08
	0.008	44.8±0.1	43.0	449±4	250±5	0.56±0.02
P_{con}	0.134	49.4±0.3		399±10	267±2	0.67±0.02
	0.013	42.8±2.0	42.1	369±30	212±36	0.57±0.19
P_{sb}	0.120	46.0±0.2		411±5	280±9	0.68±0.02
	0.0125	43.0±0.3	39.4	503±7	250±5	0.50±0.02
P_{slac}	0.110	43.2±0.1		403±3	292±3	0.72±0.02
	0.012	39.0±0.2	37.0	413±4	330±6	0.73±0.02
P_{N25}	0.119	39.5±0.1		356±1	239±3	0.67±0.01
	0.011	34.5±0.5	31.6	428±86	131±3	0.31±0.06

[a] Calculated values from Eq. (5) in the text.

Table 6
Thermodynamic comparison of the transcription "bubble" promoter duplex dissociation from DSC with association from ITC

Promoter	Concentration	$\Delta_d H$	ITC $-\Delta_b H$[a]	Cal.[b] $\Delta_b G^o$ (298 K)	ITC $-\Delta_b G^o$ (298 K)
	mM	kJ mol^{-1}		kJ mol^{-1}	
P_{tac}	0.120	328±11	302±29	49.4±1.7	42.0±0.4
P_L	0.134	231±4	346±6	46.2±1.7	41.7±0.2
P_{sb}	0.120	280±9	320±9	42.9±1.4	41.0±0.4
P_{slac}	0.110	292±3	341±5	41.2±0.4	38.6±0.2
P_{con}	0.134	267±2	272±5	44.0±0.4	38.6±0.3
P_{bla}	0.112	273±7	462±48	47.4±0.9	38.4±0.2
P_{N25}	0.119	239±3	266±22	36.9±0.3	33.6±0.2

[a] The ITC binding enthalpies are average values of the binding enthalpies at 25 °C, 30 °C, and 35 °C.
[b] The DSC free energy changes at 25 °C are extrapolated values via Eqs. (4a) and (4b) in the text using the DSC transition enthalpy value.

Eq. (5) and the transition enthalpies are also presented in Table 5 and are only in fair agreement with the experimental values at the lower DNA concentrations. The DSC results are compared to the ITC results in Table 6. The ITC binding enthalpies and the DSC dissociation enthalpies are the same for P_{tac}, P_{con}, and P_{N25} but less than 48% higher for P_L and P_{bla}, and less than 14% higher for P_{slac} and P_{sb}. The extrapolated DSC dissociation free energy changes are less than 8% higher than the ITC binding free energy changes for P_L, P_{sb}, P_{slac}, and P_{N25}, less than 13% higher for P_{tac} and P_{con}, and 20% higher for P_{bla}. The large error in the extrapolated DSC free energy changes arises from the large uncertainties in the DSC transition enthalpies employed in Eqs. (4a) and (4b) for the extrapolation. The larger differences between the ITC and extrapolated DSC free energy changes are for the weaker affinity binding duplexes, P_{con}, P_{bla}, and P_{N25}.

4. Discussion

The binding thermodynamics of the mutated *syncon* promoters show that the promoter binding affinities to RNAP are dependent on the base sequences in the −10 bp binding region, whereas the promoter binding affinities exhibit little dependence on the base sequences in the −35 bp binding region. This is especially apparent by the order of magnitude reduction in the binding constant upon mutation of two separated bases in the −10 bp region of the *syncon B* promoter and by the reduction in the binding constant of the *synlac* promoter with mutation of two adjacent bases in the −10 bp region. The promoter–RNAP binding reactions are all enthalpically-driven, arising out of hydrogen bonding and van der Waals interactions between the promoter bases and the amino acid residues of the RNAP, with some negative contributions from a decrease in the entropy upon binding. Entropic contributions upon binding would result from the release of counter-ions from the promoter phosphate backbone with a commensurate increase in the binding affinity, from a decrease in the translational/rotational degrees of freedom of the RNAP and the promoter, and from changes in hydration [28]. For a number of protein–DNA binding interactions, for example, it has been observed that water is highly ordered in an AT-rich minor groove of DNA so that its removal upon protein binding results in an increase in the binding entropy [28]. Enthalpy–entropy compensation, where changes in the binding enthalpy are compensated by changes in the binding entropy, has been observed isothermally in a number of DNA–protein binding reactions [29]. This is also observed in Table 2 for the binding of *syncon*, *synlac*, and *syncon A* promoters to RNAP at 25 °C and suggests an important role for water molecules in the promoter–RNAP binding reactions. Any large conformational changes in the RNAP or the promoter in the promoter–RNAP complex would substantially reduce the exothermicity of the binding reaction since such conformational changes are endothermic in nature. However, the reduction in the exothermicity of the binding enthalpy would be compensated by an increase in the binding entropy resulting from the release of water molecules to the bulk solvent during the conformational change [29]. A conformational change in the promoter–RNAP complex upon its formation is implied in the large binding heat capacity change of $\Delta_b C_p = -10.7 \pm 1.9$ kJ mol^{-1} K^{-1} for the *syncon* promoter. Contributions to a negative heat capacity change would also result from extensive dehydration of a polar group on the RNAP as well as from dehydration of a major groove of the promoter upon RNAP–promoter binding [28]. Identification of the nature of the conformational change could be derived from comparison of the DSC results on the thermal unfolding of RNAP in the presence and absence of the *syncon* promoter.

The DSC scans of the RNAP alone exhibit two thermal unfolding transitions at different transition temperatures but with almost equal van't Hoff enthalpies. A high ratio of 3.2–3.5 is obtained if the average van't Hoff enthalpy is divided into the total calorimetric enthalpy for the transition. The unfolding transitions of simple globular proteins yield enthalpy ratios = 1.00, whereas more structurally complex proteins consisting of several structural sub-domains may yield several transitions at different temperatures, identified as a transition occurring for each sub-domain, or several transitions occurring at the same transition temperature [30]. In the latter case, the enthalpy ratios would be greater than 1.0, depending on how strongly the sub-domains interact. With a high ratio of 3.2–3.5 as observed for the unfolding transitions of RNAP, it appears that this high ratio results from almost independent unfolding of each of the α, α′, β, β′, and σ structural subunits of RNAP. It is also possible to analyze the transitions of RNAP as a superposition of two-state single A↔B transitions of up to four thermodynamic domains of the RNAP. Again, these thermodynamic domains may be identified with the σ, α, α′, β′ and β structural subunits of unligated RNAP. A single thermal unfolding transition is observed in DSC scans of the RNAP–promoter complex again with high $\Delta_{trs}H/\Delta_{trs}H_{vH}$ ratios averaging 4.3, indicating the existence of a superposition of two-state A↔B transitions of at least four thermodynamic domains of RNAP. These thermodynamic domains may be identified as the almost independent unfolding of the σ α, α′, β′ and β structural subunits of the RNAP–promoter complex (although upon binding to the promoter, the σ subunit dissociates from the complex, this subunit would still be present in the sample). Similar independence of the structural subunits of RNAP is observed on a higher evolutionary scale in the assembly of the analogous transcription complexes with up to 50 co-factors in eukaryotic transcription. A single transition observed at 60 °C in DSC scans of the RNAP–promoter complex is predictable if the original high temperature transition is unaffected by promoter binding and the subunits unfolding at the lower temperature transition are thermally stabilized via promoter binding specifically to these units. The thermal stabilization will cause the low temperature transition to shift to a higher temperature upon promoter binding to the degree predicted by Eqs. (4a) and (4b). The σ, β, and β′ subunits are the subunits of RNAP that would interact with the promoter. If this is correct, then any conformational change upon promoter binding to RNAP, implied by the large negative heat capacity change, is not detectable by DSC or the conformational change is the bending of the promoter upon binding to RNAP as observed by scanning force microscopy [5]. Bending of the promoter, particularly at a major groove, would result in dehydration of the major groove and a negative heat capacity change [28].

Localized melting of a subset of DNA sequences in the promoter occurs near the transcription start point to form a transcription bubble as the initial closed form of the promoter–RNAP complex isomerizes to the open form. In Table 6, the free energy changes required to melt the promoter subsets range from $\Delta_d G^o = 33.6 \pm 0.2$ to 36.9 ± 0.3 kJ mol^{-1} for the P_{N25} bubble sequence to $\Delta_d G^o = 42.0 \pm 0.4$ to 49.4 ± 1.7 kJ mol^{-1} for the P_{tac} bubble sequence at 25 °C, which has the same sequence as in the *syncon* promoter in Fig. 1. At the lower concentrations of the promoters in the cell, the thermal stabilities of the transcription bubble subsets are lower so that the free energy requirements for melting of the short DNA duplex subset to form the transcription

bubble are lower, as indicated by the DSC results at the dilute concentrations of the bubble duplexes in Table 5. The dissociation results are for the short duplex transcription bubble sequences, which were designed from the transcription start point to the −12 bp promoter sequence, and are only part of the full length promoter. It is not known how the remaining promoter duplex contributes to the formation of the transcription bubble. Bending of the promoter is represented to begin at −12 bp from the transcription start point [4] and this may weaken the effect of the remainder promoter upstream sequences on the thermodynamic stability of the transcription bubble duplexes. In addition, further justification of the use of shorter DNA duplexes to mimic the formation of the transcription bubble is that shorter 14 bp promoter duplex fragments consisting of only the −10 consensus sequence underwent melting at temperatures above 14 °C when bound to RNAP [10]. Less than 20% of the RNAP consisting of amino acid residues 1 to 314 of the β subunit and 94–507 of the σ subunit were required to melt an extended −10 promoter [10]. On this basis the dissociation thermodynamics of the short promoter duplexes P_{tac}, P_L, P_{bla}, P_{con}, and P_{N25} determined from the DSC results are important to show that the free energy of formation of the transcription bubble depends on the sequence by 33.6 to 49.4 kJ mol^{-1}.

In summary, it appears that the free energy required for the initiation of transcription of a promoter into messenger RNA arises mainly from the exothermic binding energy of the promoter to the RNAP. It does not appear from the DSC results on RNAP and the RNAP–promoter complex that the large heat capacity change upon promoter binding to RNAP can be attributed to a conformational change in the RNAP upon promoter binding. The RNAP subunits appear to exhibit minimal interaction and, thus, unfold almost as independent entities, similar to eukaryotic transcription initiation complexes, which are composed of up to 50 transcription factors. The process of binding ($\Delta_b G^o$), nucleation, and melting ($\Delta_d G^o$) to form the transcription bubble are driven by the binding free energy change [3]. In order for the initiation of transcription to proceed including isomerization from the closed promoter–RNAP complex to the open form ($\Delta_i G^o$) and the formation of the transcription bubble ($\Delta_d G^o$), the net free energy changes

$$\Delta_b G^o + \Delta_d G^o + \Delta_i G^o < 0 \tag{7a}$$

so that,

$$\Delta_b G^o < -(\Delta_d G^o + \Delta_i G^o) \tag{7b}$$

For the *syncon* promoter where $\Delta_b G^o = -42.1 \pm 0.2$ kJ mol^{-1} and $\Delta_d G^o = 42.0 \pm 0.2$ kJ mol^{-1} at 0.120 mM *syncon* promoter and if the concentration of the *syncon* promoter in the cell is 0.120 mM, then $\Delta_i G^o = 0$. However, the promoter concentration in the cell is much lower. For example using a 0.01 μM promoter concentration based on 200 nucleotide molecules in an *E. coli.* cell volume of 33×10^{-15} L [31] and Eq. (5), then $\Delta_d G^o$ would be reduced from 42.1 ± 0.2 kJ mol^{-1} to ~19 kJ mol^{-1}. This would allow for the condition that

$$\Delta_i G^o < 23 \text{ kJ mol}^{-1} \tag{8}$$

and the initiation of transcription would proceed with the formation of the transcription bubble. The subsequent processes of RNA chain initiation, elongation, and termination would involve release and hydrolysis of diphosphate from the ribonucleoside triphosphate reactants as the promoter is transcribed into messenger RNA.

Certain commercial materials, instruments, and equipment are identified in this manuscript in order to specify the experimental procedure as completely as possible. In no case does such identification imply a recommendation or endorsement by the National Institute of Standards and Technology nor does it imply that the materials, instruments, or equipment identified is necessarily the best available for the purpose.

References

[1] S. Lisser, H. Margalit, Compilation of *E. coli* mRNA promoter sequences, Nucleic Acids Res. 21 (1993) 1507–1516.
[2] W.R. McClure, Rate-limiting steps in RNA chain initiation, Proc. Natl. Acad. Sci. 77 (1980) 5634–5638.
[3] R.M. Saecker, O.V. Tsodikov, K.L. McQuade, P.E. Schlax, M.W. Capp, M.T. Record, Kinetic studies and structural models of the association of *E. coli* σ^{70} RNA polymerase with the λPr promoter: large scale conformational changes in forming the kinetically significant intermediates, J. Mol. Biol. 319 (2002) 649–671.
[4] W.A. Rees, R.W. Keller, J.P. Vesenka, G. Yang, C. Bustamante, Evidence of DNA bending in transcription complexes imaged by scanning force microscopy, Science 260 (1993) 1646–1649.
[5] J.D. Helmann, P.L. deHaseth, Protein–nucleic acid interactions during open complex formation investigated by systematic alteration of the protein and DNA binding partners, Biochemistry 38 (1999) 5959–5967.
[6] T. Heyduk, A. Niedziela-Majka, Fluorescence resonance energy transfer analysis of *Escherichia coli* RNA polymerase and polymerase–DNA complexes, Biopolymers 61 (2002) 201–213.
[7] G. Zhang, E.A. Campbell, L. Minakhin, C. Richter, K. Severinov, S.A. Darst, Crystal structure of *Thermus aquaticus* core RNA polymerase at 3.3 Å resolution, Cell 98 (1999) 811–824.
[8] P. Cramer, D.A. Bushnell, J. Fu, A.L. Gnatt, B. Maier-Davis, N.E. Thompson, Architecture of RNA polymerase II and implications for the transcription mechanism, Science 288 (2000) 640–649.
[9] P.H. von Hippel, An integrated model of the transcription complex in elongation, termination, and editing, Science 281 (1998) 660–665.
[10] A. Niedziela-Majka, T. Heyduk, *Escherichia coli* RNA polymerase contacts outside the −10 promoter element are not essential for promoter melting, J. Biol. Chem. 280 (2005) 38219–38227.
[11] M. Brunner, H. Bujard, Promoter recognition and promoter strength in the *Escherichia coli* system, The EMBO J. 6 (1987) 3139–3144.
[12] Y.F. Chen, J.D. Helmann, DNA-melting at the *Bacillus subtilis* flagellin promoter nucleates near −10 and expands unidirectionally, J. Mol. Biol. 267 (1997) 47–59.
[13] D.A. Rowe-Magnus, G.B. Spiegelman, DNA strand separation during activation of a developmental promoter by the *Bacillus subtilis* response regulator Spo0A, Proc. Natl. Acad. Sci. U.S.A. 95 (1998) 5305–5310.
[14] T. Aoyama, M. Takanami, E. Ohtsuka, Y. Taniyama, R. Marumoto, H. Sato, M. Ikehara, Essential structure of *E. coli.* promoter: effect of spacer length between the two consensus sequences on promoter function, Nucleic Acids Res. 11 (1983) 5855–5864.
[15] E. Heyduk, K. Kuznedelov, K. Severinov, T. Heyduk, A consensus adenine at position −11 of the nontemplate strand of bacterial promoter is important for nucleation of promoter melting, J. Biol. Chem. 281 (2006) 12362–12369.
[16] P.A. Lowe, D.A. Hager, R.R. Burgess, Purification and properties of the sigma subunit of *Escherichia coli* DNA-dependent RNA polymerase, Biochemistry 18 (1979) 1344–1352.
[17] R.R. Burgess, J.J. Kendrick, A procedure for the rapid, large-scale purification of Escherichia coli DNA-dependent RNA polymerase involving polyamine P precipitation and DNA-cellulose chromatography, Biochemistry 14 (1975) 4634–4638.
[18] X. Zhang, Y. Zhou, Y.W. Ebright, R.H. Bright, Catabolite gene activator protein (CAP) is not an "acidic activating region" transcription activator protein, J. Biol. Chem. 267 (1992) 8136–8139.
[19] J. Sambrook, E.F. Fritsch, T. Maneates, Molecular Cloning: A Laboratory Manual, 2nd EdCold Spring Harbor Laboratory, Cold Spring Harbor, New York, 1989 P. E5.
[20] S. Krueger, S. Gregurick, Y. Shi, S. Wang, B.D. Wladkowski, F.P. Schwarz, Entropic nature of the interaction between promoter bound CRP Mutants and RNA polymerase, Biochemistry 42 (2003) 1958–1968.
[21] W.H. Kirchhoff, Exam: A Two-state Thermodynamic Analysis Program, NIST Tech. Note 1401, U.S. Government Printing Office, Washington, D.C., 1993.
[22] K.J. Breslauer, in: H-J Hinz (Ed.), Methods for Obtaining Thermodynamic Data on Oligonucleotide Transitions in Thermodynamic Data for Biochemistry and Biotechnology, Springer-Verlag, New York, 1986.
[23] F.P. Schwarz, Interaction of cytidine 3′-monophosphate and uridine 3′-monophosphate with ribonuclease a at the denaturation temperature, Biochemistry 29 (1988) 880–885.
[24] S.P. Manly, K.S. Matthews, J.M. Sturtevant, Thermal-denaturation of the core protein of lac repressor, Biochemistry 24 (1985) 3842–3846.
[25] F.P. Schwarz, S. Robinson, J.M. Butler, Thermodynamic comparison of PNA/DNA and DNA/DNA hybridization reactions at ambient temperatures, Nucleic Acids Research 27 (1999) 4792–4800.
[26] J. Zhou, S.K. Gregurick, S. Krueger, F.P. Schwarz, Conformational changes in single-stranded DNA as a function of temperature by SANS, Biophys. J. 90 (2006) 1–8.
[27] B.E. Lang, F.P. Schwarz, Thermodynamic dependence of DNA/DNA and DNA/RNA hybridization reactions on temperature and ionic strength, Biophysical Chemistry 131 (2007) 96–104.
[28] P.L. Privalov, A.I. Dragan, C. Crane-Robinson, K.J. Breslauer, D.P. Remta, C.A.S.A. Minetti, C.A.S.A. Minetti, What drives proteins into the major or minor grooves of DNA, J. Mol. Biol. 365 (2007) 1–9.
[29] L. Jen-Jacobson, L.E. Engler, L.A. Jacobson, Structural and thermodynamic strategies for site-specific DNA binding proteins, Structure 8 (2000) 1015–1023.
[30] P.L. Privalov, Stability of proteins, proteins which do not present a single cooperative system, Advances in Protein Chemistry 35 (1982) 1–104.
[31] B. Alberts, D. Bray, J. Lewis, M. Raff, K. Roberts, J.D. Watson, Molecular Biology of the Cell, Garland Publishing Co., New York, 1983.